DE GRUYTER
OPEN

Contributions to Geophysics and Geodesy Vol. 47/1, 2017 (69–80)

Calculation of temperature distribution and rheological properties of the lithosphere along Profile 1 passing through Aswan

Anwar H. RADWAN[1], Jana DÉREROVÁ[2], Miroslav BIELIK[2,3], Barbora ŠIMONOVÁ[3], Igor KOHÚT[2]

[1] National Research Institute of Astronomy and Geophysics, Department of Geodynamics, EL Marsad Street 1, Helwan, Cairo, Arab Republic of Egypt;
e-mail: radwan99@yahoo.com

[2] Earth Science Institute, Slovak Academy of Sciences,
Dúbravská cesta 9, P.O. Box 106, 840 05 Bratislava, Slovak Republic;
e-mail: geofjade@savba.sk

[3]Department of Applied and Environmental Geophysics, Faculty of Natural Sciences, Comenius University,
Mlynská dolina, Ilkovičova 6, 842 48 Bratislava, Slovak Republic;
e-mail: bielik@fns.uniba.sk

Abstract: The 2D integrated geophysical modelling approach has been used to determine the temperature distribution in the lithosphere along the profile passing through Aswan. Based on the temperature model and the rheological parameters, we have calculated strength distribution in the lithosphere for the studied profile. The strength envelopes have been calculated for both compressional and extensional regimes. Our results indicate that the strength is constant along the whole length of the profile passing through the Nubia plain. The largest strength can be observed within the upper crust which allows us to assume rigid deformation in this part of the lithosphere, with compressional processes predominant. Towards the lower crust and upper mantle, strength values rapidly decrease for both regimes, suggesting ductile deformations in the lower part of the lithosphere.

Key words: Aswan, integrated modelling, temperature, rheology, strength, compression, extension

1. Description of the investigated area

The Aswan area is structurally a part of the east Sahara Craton in NE Africa (Fig. 1). The major structural zones cutting North Africa and Ara-

doi: 10.1515/congeo-2017-0005

Brought to you by | National Sciences Library Chinese Academy of Science
Authenticated
Download Date | 12/19/17 10:18 AM

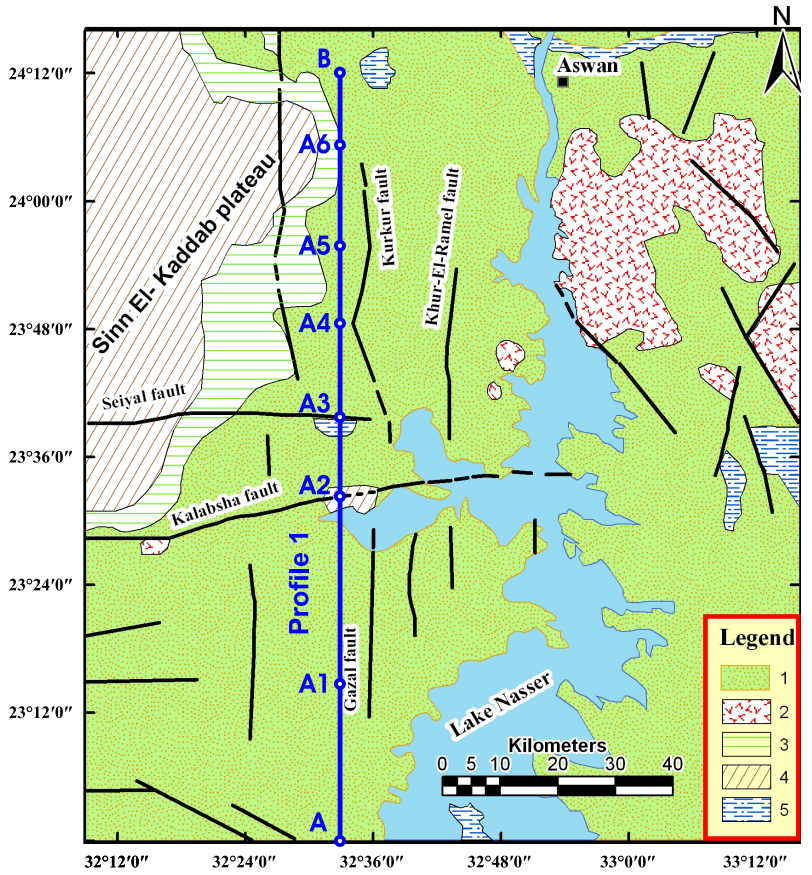


Fig. 1. Geology of Aswan and location of Profile 1 (modified after the *Egyptian Geological Survey and Mining Authority (EGSMA), 1981; Woodward-Clyde Consultant (WCC), 1985; Azeem et al., 2014*).

bia have been studied by many geologists (e.g., *Nagy et al., 1976; Davies, 1984; Schandelmeier et al., 1987; Bernau and Franz, 1987*). The structural pattern of the Aswan area is controlled by regional basement rock uplift and regional faulting (*Issawi 1969, 1971, 1978*). The structural high that has formed east of the River Nile has resulted in outcrops of Precambrian basement rocks in the Aswan hills. On the western side of this broad north to northwest-trending upward, the Nubia Formation and overlying stratigraphic units have been gently titled toward the west and northwest.

Brought to you by | National Sciences Library Chinese Academy of Science
Authenticated
Download Date | 12/19/17 10:18 AM

In the Aswan area four geological and geomorphological features can be distinguished (Fig. 1). From east to west are the Aswan Hills, the Nile River Valley, the Nubian Plain, and the Sinn-el Kaddab Plateau. The latter two are within the area referred to as the Western Desert (*Geological Survey and Mining Authority (EGSMA), 1981; Woodward-Clyde Consultant (WCC), 1985; Azeem et al., 2014*).

The Aswan Hills are located along the East side of the Nile Valley and extend from the vicinity of Aswan southwards, along the eastern bank of Lake Nasser, in parallel to the southern limit of the area. The Aswan hills are characterized by rugged topography produced by a dense, intricate system of steep valleys. The Hills reach elevations of 200 to 300 m and represent remnants of ancient erosion surfaces possibly formed as early as the middle Tertiary (*Butzer and Hansen, 1968*). They are composed of pre-Cambrian basement rocks, which are exposed within the hills along the crest of the uplift. The flanks of the basement complex are clastic sedimentary rocks of very gently dipping sandstone, shales, and ferruginous sandstone.

The Nile River valley is located along the western edge of the Aswan Hills; the modern Nile valley occupies a gorge that was incised during the late Miocene, when the base level of the proto-Nile River fell as a result of evaporation of the Mediterranean Sea. In the Aswan area, remnants of the upper part of the ancient canyon form the present narrow valley and steep-sided bedrock canyon that have been down cut into both the sandstone of the Nubia Formation and the Precambrian basement complex. South of the High Dam, this canyon is now inundated by Lake Nasser. Where the basement of the canyon is formed by the Precambrian crystalline rocks the channel is narrow and deep. On the other hand the areas where the basement consists of the Nubia Formation sandstone the channel is wide and shallow.

The Nubia plain extends from the Nile in the east to the Sinn el-Kaddab scarp in the west. The surface of this plain is about l00 to 200 m above the Nile floodplain in the Nile valley. Near its western margin, the surface of the plain begins to rise and merges with the steep, east-facing slopes of the Sinn el-Kaddab Plateau escarpment. The bedrock of the Nubia Plain consists primarily of Nubia Formation and overlying Late Cretaceous Dakhla Formation. The Nubia Formation underlies the central and eastern portion of the plain. The Dakhla Formation underlies much of the western portion

Brought to you by | National Sciences Library Chinese Academy of Science
Authenticated
Download Date | 12/19/17 10:18 AM

of the plain, as well as the lower slope of the escarpment of the Sinn el-Kaddab Plateau. Quaternary deposits are absent over much of the Nubia Plain. Only near the escarpment of the Sinn el-Kaddab Plateau are older Quaternary deposits extensive enough to be of use in evaluating the degree of Quaternary activity along the faults of the Nubia Plain.

The Sinn el-Kaddab Plateau is a vast limestone-capped tableland that extends over the western edge of the study area. The eastern margin of this plateau is a steep, east-facing escarpment called the Sinn el-Kaddab escarpment. The base of the escarpment consists of the Dakhla Formation, which is overlain by the Kurkur and Garra Formations. The Kurkur Formation is a marine limestone, shale, sandstone, and conglomerate of Palaeocene age (*Issawi, 1969*). The unconformably overlying Garra Formation is a sequence of late Palaeocene to early Eocene limestone with shale and marl intercalations (*Issawi, 1969*). Farther west, a lithologically similar limestone formation, the Dungul Formation, overlies the Garra Formation and caps the plateau surface. The Dungul Formation is early to middle Eocene in age (about 45 to 50 Ma). Quaternary deposits are fairly rare on the plateau surface, and consist primarily of sand dunes. The structure of the plateau is an essentially flat-lying sequence of strata, which is interrupted by several faults with W-E directions (the Seiyal and Kalabsha faults) and N-S trend (the faults: Gazal, Abu Dirwa, Gabel el-Barqa, Kurkur, Khur-El-Ramel).

2. Computing method

The lithospheric structure along Profile 1 (Fig. 1) has already been modelled using the 2D integrated geophysical modelling method that combines the interpretation of surface heat flow, geoid, gravity, and topography data for the determination of the lithospheric thermal structure (Fig. 2). A detailed description of the method can be found in *Zeyen and Fernàndez (1994)*. The full modelling results for profile 1 have been described in *Radwan et al. (2006)*. Based on the determined temperature field in the lithosphere, we can calculate the yield strength for a given distribution of rheological rock parameters. The strength is defined as the minimum of brittle and ductile strength at each point. For brittle strength calculation we have assumed that deformation occurs according to the frictional sliding law given by *Byerlee (1978)*:

Brought to you by | National Sciences Library Chinese Academy of Science
Authenticated
Download Date | 12/19/17 10:18 AM

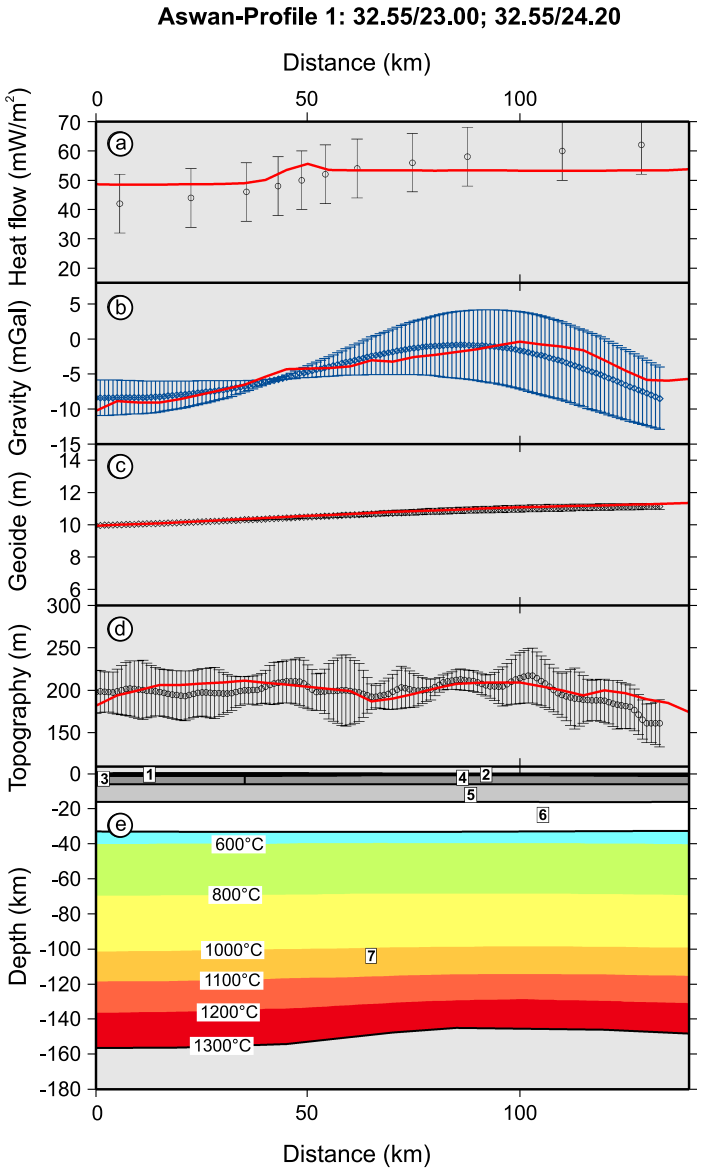


Fig. 2. Lithospheric model along profile 1. (a) Surface heat flow, (b) free air gravity anomaly, (c) topography, (d) geoid with dots corresponding to measured data with uncertainty bars and solid lines to calculated values. Numbers in (e) correspond to material number in Table 1b (*Radwan et al., 2006*).

Brought to you by | National Sciences Library Chinese Academy of Science
Authenticated
Download Date | 12/19/17 10:18 AM

$$\sigma_{brittle} = \alpha \rho g z (1 - \lambda) ,$$

where $\sigma_{brittle}$ is brittle failure function [Pa], parameter $\alpha = R - 1/R$ is valid for normal faulting, $\alpha = R - 1$ for thrust faulting, $\alpha = R - 1/[1 + \beta(R - 1)]$ for strike-slip faulting. Parameter $R = [(1 + f_s^2)^{1/2} - f_s]^{-2}$ depends on coefficient of static friction f_s, λ represents the hydrostatic pore fluid factor, ρ is material density [kg m^{-3}], g is acceleration of gravity [m s^{-2}], z is depth [m], β is extension factor.

Ductile strength is calculated assuming power-law creep deformation given as (*Lynch and Morgan, 1987*)

$$\sigma_{creep} = \left(\frac{\dot{\varepsilon}}{A_p} \right)^{1/n} \exp \left[\frac{E_p}{nRT} \right],$$

where σ_{creep} is power law creep function [Pa], $\dot{\varepsilon}$ denotes strain rate [s^{-1}], A_p is Dorn constant, n is power law exponent, E_p is power law activation energy [kJ mol^{-1}], R is universal gas constant [8.314 J mol^{-1}K^{-1}], T is temperature [K].

3. Results

We have calculated temperature distribution for a given model along profile 1 (Fig. 3), where the lower limit of the model corresponds to the 1300 °C

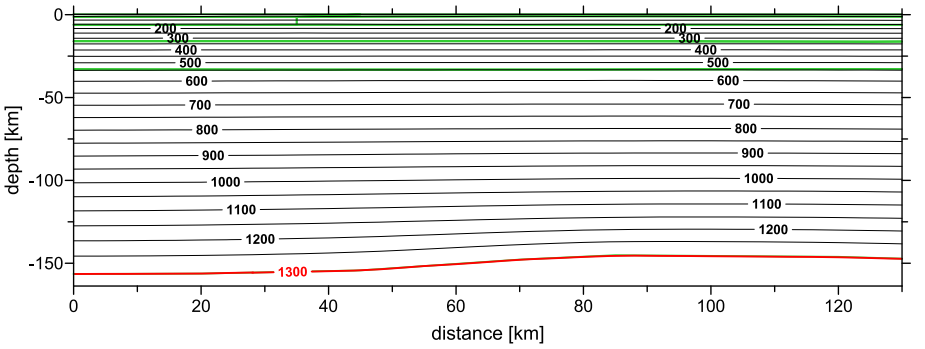


Fig. 3. Lithospheric temperature temperature distribution for profile 1. Isolines every 100 °C. The bottom of the model corresponds to the 1300 °C isotherm.

Brought to you by | National Sciences Library Chinese Academy of Science
Authenticated
Download Date | 12/19/17 10:18 AM

isotherm. The resulting temperature field is determined by the effect of the heat sources and background heat flow density from the lower mantle. The reliability of the temperature model normally depends on the accuracy and density of measurements of the surface heat flow density but since our lithological model is controlled by calculation of free air anomaly, the topography and geoid reliability of the model increases greatly.

Based on the rheological parameters shown in Table 1a and Table 1b, we have calculated strength distribution in the lithosphere for the studied profile. Fig. 4 shows vertically integrated compressional and extensional strength calculated along profile 1. Figs. 5 and 6 show the calculated yield strength contour plot for compressional and extensional deformation. In our

Table 1a. General properties used for calculation of rheological model.

Definition	**Parameter**	**Value**
Gravity acceleration [ms^{-2}]	g	9.806
Universal gas constant [$\mathrm{J\,mol\,K}^{-1}$]	R	8.314
Temperature at the base of the lithosphere [°C]	T_m	1300
Static friction coefficient	f_s	0.6
Strain rate [s^{-1}]	$\dot{\varepsilon}$	10^{-15}
Hydrostatic pore fluid factor	λ	0.35

Table 1b. Thermal and rheological parameters used for modelling along transect II (after *Carter and Tsenn (1987)* and *Goetze and Evans (1979)*). HP: heat production ($\mu\mathrm{Wm}^{-3}$), TC: thermal conductivity ($\mathrm{Wm}^{-1}\mathrm{K}^{-1}$), ρ: density at room temperature ($\mathrm{kg\,m}^{-3}$), A_p: power law pre exponential constant, n: power law exponent, E_p: power law activation energy ($\mathrm{kJ\,mol}^{-1}$).

Nr.	**Unit**	**v HP**	**TC**	**Density ρ**	$\boldsymbol{A_p}$	$\boldsymbol{n}$	$\boldsymbol{E_p}$
1	Nubian sandstone 1	1.0	2.0	2100	3.16E−26	3.30	186
2	Nubian sandstone 2	2.5	2.5	2100	3.16E−26	3.30	186
3	Weathered granite 1	2.0	2.0	2690	3.16E−26	3.30	186
4	Weathered granite 2	2.5	2.0	2690	3.16E−26	3.30	186
5	Consolisate granite (upper crust)	1.0	1.9	2750	3.16E−26	3.30	186
6	Lower crust	0.2	2.0	2930	6.31E−20	3.05	276
7	Mantle lithosphere	0.05	3.4	3205	7.94E−18	4.50	535

Brought to you by | National Sciences Library Chinese Academy of Science
Authenticated
Download Date | 12/19/17 10:18 AM

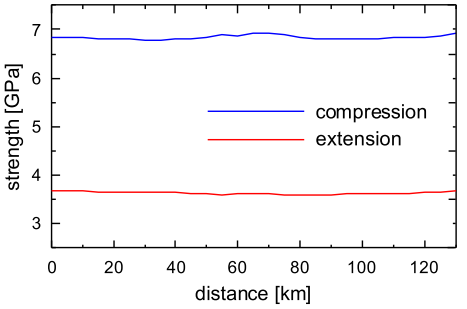


Fig. 4. Vertically integrated compressional (full line) and extensional (dotted line) strength calculated along the profile.

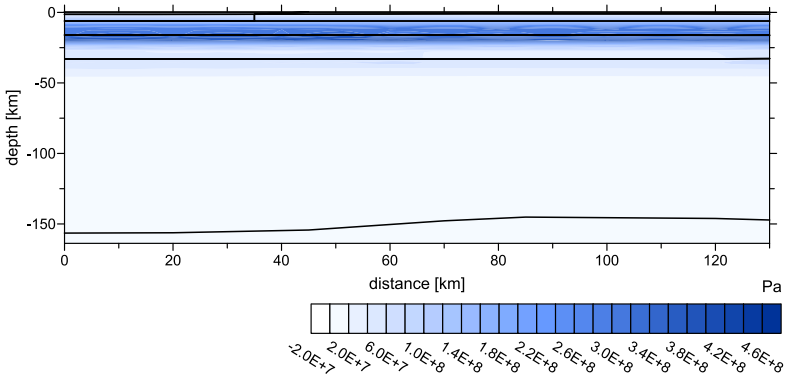


Fig. 5. Yield strength contour plot for compressional deformation calculated along profile 1 at a strain rate of 10^{-15} s^{-1}.

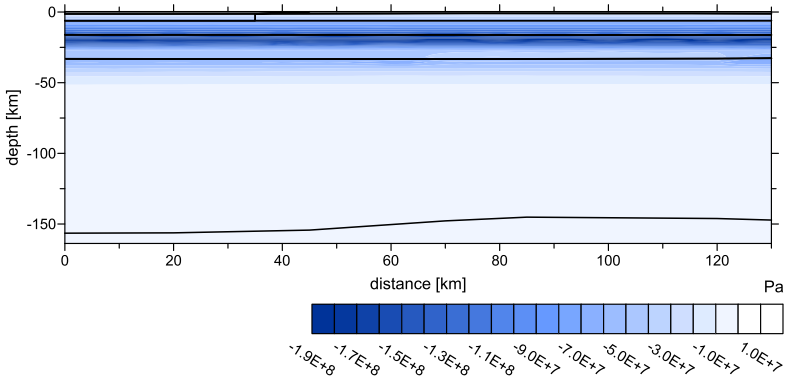


Fig. 6. Yield strength contour plot for extensional deformation calculated for along profile 1 at a strain rate of 10^{-15} s^{-1}.

Brought to you by | National Sciences Library Chinese Academy of Science
Authenticated
Download Date | 12/19/17 10:18 AM

calculations we adopted a strain rate 10^{-15} s^{-1}, which is commonly observed in compressional and extensional settings (*Carter and Tsenn, 1987*). The strength envelopes have been calculated for both compressional and extensional regimes. Figs. 7a, 7b and 7c show strength distribution for selected lithospheric columns along the profile 1 in Aswan.

4. Conclusions

The calculated results related to the vertically integrated compressional and extensional strength along Profile in Aswan 1 (Fig. 4) shows that the strength is constant along the whole length of profile passing through the Nubia plain.

Analysis of the yield strength contour plot (Figs. 5 and 6), and vertical strength distribution for different lithospheric columns (A1–A6) for compressional and extensional deformation, (Fig. 7) calculated along the Aswan profile, indicates the largest strength can be observed within the

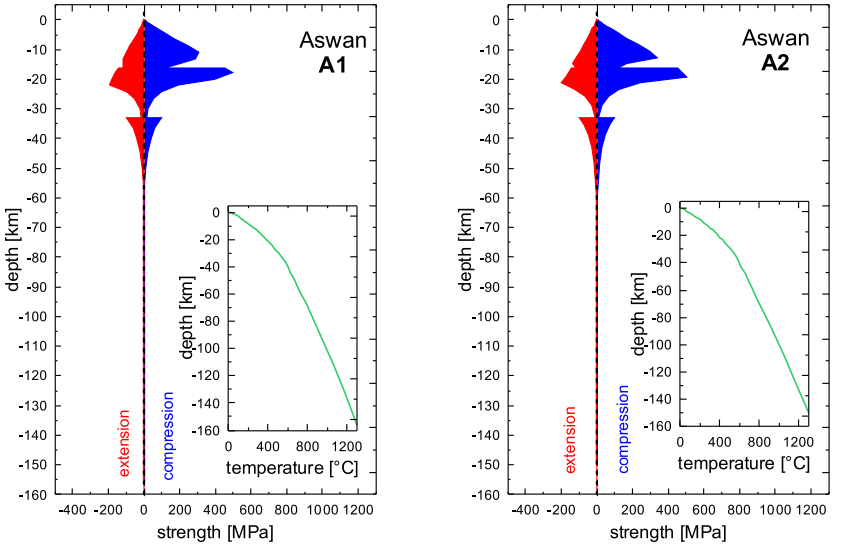


Fig. 7a. Vertical strength distribution for different lithospheric columns A1 and A2 along profile 1. Negative and positive values correspond to extensional and compressional strength respectively.

Brought to you by | National Sciences Library Chinese Academy of Science
Authenticated
Download Date | 12/19/17 10:18 AM

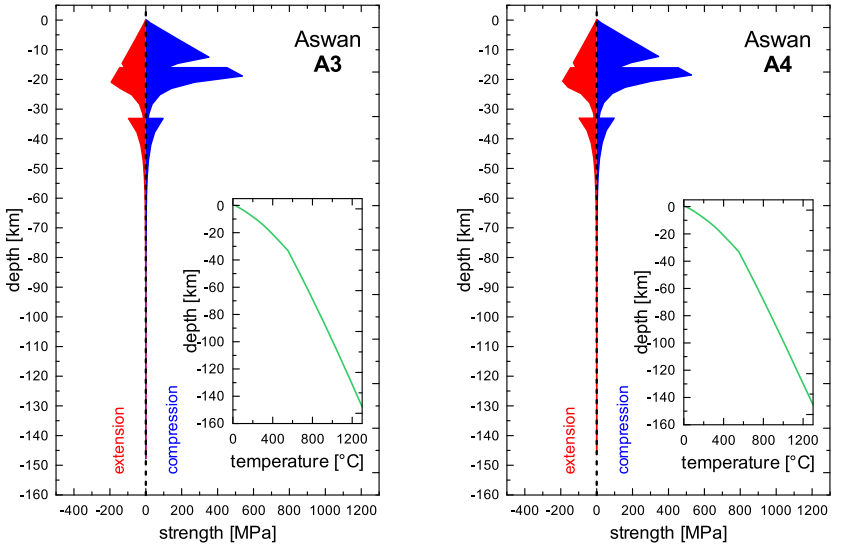


Fig. 7b. Vertical strength distribution for different lithospheric columns A3 and A4 along profile 1. Negative and positive values correspond to extensional and compressional strength respectively.

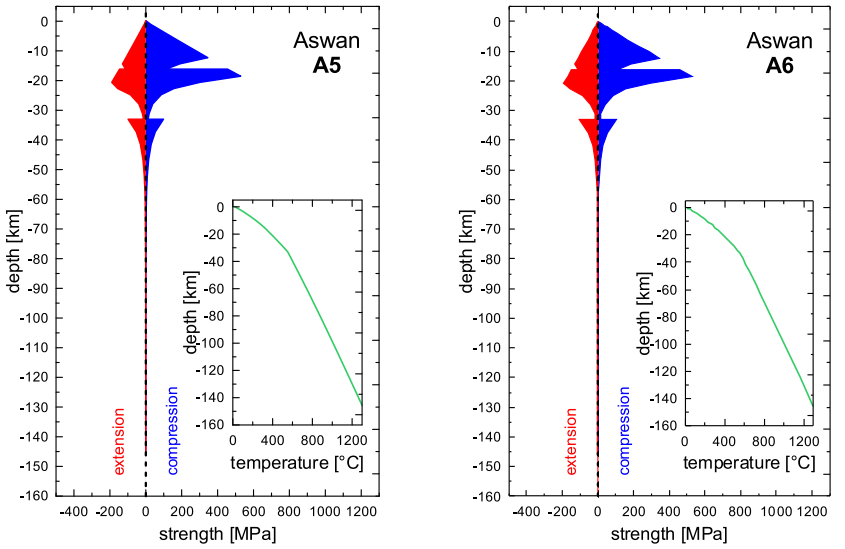


Fig. 7c. Vertical strength distribution for different lithospheric columns A5 and A6 along profile 1. Negative and positive values correspond to extensional and compressional strength respectively.

Brought to you by | National Sciences Library Chinese Academy of Science
Authenticated
Download Date | 12/19/17 10:18 AM

upper crust with the maximum (400–500 MPa) on the boundary between the upper and lower crust. This means that in the upper crust, rigid deformation is dominant in the whole area. The strength in the lower crust significantly decreases and completely diminishes within the upper mantle. That indicates ductile deformation in this lower part of the lithosphere.

Acknowledgements. This research was supported by the Slovak Research and Development Agency under the contracts No. APVV-16-0146, APVV-16-0482, APVV-0724-11, and Slovak Grant Agency VEGA, grants 2/0042/15, 1/0141/15 and 1/0462/16. Authors are grateful to Prof. Hermann Zeyen (Laboratoires IDES, Université Paris-Sud XI) for permission to use 2D integrated modelling software.

References

Azeem M. A., Mekkawi M., Gobashy M., 2014: Subsurface structures using a new integrated geophysical analysis, South Aswan, Egypt. Arab. J. Geosci., **7**, 12, 5141–5157, doi: 10.1007/s12517-013-1140-x.

Bernau R., Franz G., 1987: Crystal Chemistry and Genesis of Nb-, V-, and Al-rich Metamorphite Titanite from Egypt and Greece. Canadian Mineralogist, **25**, 695–705.

Butzer K., Hansen C., 1968: Desert and River in Nubia. Madison, University of Wisconsin Press (1968), 395–432.

Byerlee J., 1978: Friction of rocks. Pure Appl. Geophys., **16**, 1, 615–626.

Carter N. L., Tsenn M. C., 1987: Flow properties of continental lithosphere. Tectonophysics, **136**, 27–63.

Davies F. B., 1984: Strain analysis of wrench faults and collision tectonics of the Arabian-Nubian shield. J. Geol., **92**, 1, 37–53.

Egyptian Geological Survey and Mining Authority (EGSMA), 1981: Geological map of Egypt, Ministry of Industrial and Mineral Resources.

Goetze C., Evans B., 1979: Stress and temperature in the bending lithosphere as constrained by experimental rocks mechanics. Geophys. J. R. Astron. Soc., **59**, 3, 463–478, doi: 10.1111/j.1365-246X.1979.tb02567.x.

Issawi B., 1969: The geology of Kurkur-Dungul area. Geological Survey of Egypt, Paper 46, 102p.

Issawi B., 1971: Geology of Darb El Arbain area, Western Desert: Egypt. Geol. Survey Ann., **1**, 53–92.

Issawi B., 1978: Geology of Nubia west area, Western Desert. Ann. Geol. Survey Egypt, **8**, 237–253.

Lynch H. D., Morgan P., 1987: The tensile strength of the lithosphere and the localisation of extension. Continental Extension Tectonics, Ed.: M. P. Coward, J. F. Dewey, P. L. Hancock. Geol. Sec., Spec. Publ., London, **28**, 53–65.

Brought to you by | National Sciences Library Chinese Academy of Science
Authenticated
Download Date | 12/19/17 10:18 AM

Nagy R. M., Ghuma M. A., Rogers J. J., 1976: A crustal suture and lineament in North Africa. Tectonophysics, bf 31, 3-4, T67–T72.

Radwan A. H., Bielik M., Dérerová J., Kohút I., Issawy E., 2006: Determination of the lithospheric structure along profile I in Aswan area: 2-D integrated geophysical modeling. Al-Azhar Bull. Sci., **17**, 2, 23–33.

Schandelmeier H., Richter A., Harms U., 1987: Proterozoic deformation of the East Saharan Craton in Southeast Libya, South Egypt and North Sudan. Tectonophysics, **140**, 2-4, 233–246.

Woodward-Clyde Consultant (WCC), 1985: Identification of earthquake sources and estimation of magnitudes and recurrence intervals. Internal Report. High and Aswan Dam Authority, Egypt, 135p.

Zeyen H., Fernàndez M., 1994: Integrated lithospheric modeling combining thermal, gravity and local isostasy analysis: application to the NE Spanish Geotransect. J. Geophys. Res., **99**, B9, 18089–18102, doi: 10.1029/94JB00898.

Brought to you by | National Sciences Library Chinese Academy of Science
Authenticated
Download Date | 12/19/17 10:18 AM